Metal Atom Intercalation: Calculations and Applications

Bryan Kim, Keya Joy

EE421 Quantum Mechanics

DEPARTMENT OF ELECTRICAL ENGINEERING, UNIVERSITY OF WASHINGTON, SEATTLE, WA, 98195

I. INTRODUCTION

Graphene has been at the forefront of materials research due to several of its properties, including malleable electronic properties, stability, and high intrinsic electron mobility [1][2]. The study of 2D materials is at the crossroads of pure math, quantum mechanics, and engineering applications. Intercalation refers to the deposition of metal atoms into a substrate, and diffusion refers to the subsequent detachment of these atoms. This process has been shown to alter graphene's doping level and band structure [3], but the lower-level details are not studied as much. In this paper, we will begin with an overview of the governing physics equations, and then extensions and approximations using Density Functional Theory. Using the Nudged Elastic Band method, we calculate the minimum energy pathway of a metal atom through a defect in a graphene monolayer. After discussing the results and comparing them with literature, we explore two main applications of this research: tunable semiconductors and lithium-ion batteries.

II. QUANTUM CONCEPTS

A. Schrodinger's Equation and Density Functional Theory

Schrodinger's equation (1), which describes the waveform of a particle, is fundamental to our understanding of quantum mechanics.

$$i\hbar\frac{\partial}{\partial t}\Psi(x,t) = \left[-\frac{\hbar^2}{2m}\frac{\partial^2}{\partial x^2} + V(x,t)\right]\Psi(x,t) \tag{1}$$

where $\hbar^2$ is the reduced Planck's constant, m is the mass of the particle, V is the potential energy and Ψ is a wavefunction both as functions of position and time.

Throughout this course, the single-particle Schrodinger equation has been a cornerstone in describing the wave-like behavior of particles. However, this equation falls short when it comes to describing systems with multiple bodies, so we need to extend this framework. Then comes the Hohenberg-Kohn theorem, which states that a material's ground-state properties are a functional – a mapping from function to function – of the electron density [4]. This is the basis for solving the Schrodinger equation, which speeds up computation.

(2) is an extension of Schrodinger's Equation, which is the many-body Schrodinger equation, and the foundation for the Density Functional Theory.

$$\hat{H}\psi = \left[\hat{T} + \hat{V} + \hat{U}\right]\psi = \left[\sum_{i=1}^{N}\left(-\frac{\hbar^2}{2m_i}\nabla_i^2\right) + \sum_{i=1}^{N}V(r_i) + \sum_{i<j}^{N}U(r_i, r_j)\right]\psi = E\psi \tag{2}$$

where $\hat{T}$ is the kinetic energy, $\hat{U}$ is the electron-electron interaction energy, and $\hat{V}$ refers to the potential energy from the external field. While $\hat{T}$ and $\hat{U}$ are independent on the number of electrons, $\hat{V}$ is dependent on the configuration of the electrons. Various approaches exist for solving this equation, including the Hatree-Fock method and the Kohn-Sham equations. [5]

Hatree-Fock Method
The Hatree-Fock method is an interactive approach used to approximate the wavefunction of a multi-electron system. This process is initialized with 3D coordinates of the particles and an initial guess for the wavefunctions. These values are the input to the Fock Matrix, which contains the Hamiltonian and the electron-electron interaction terms. After the Fock matrix is constructed, the wavefunctions are updated and the matrix is recalculated iteratively until the matrix converges. Once convergence has occurred, the values are used to calculate various properties of the system, such as its energy levels and electron density. [5]

Kohn-Sham Equations
The Kohn-Sham equations approach simplifies the many-electron problem by focusing on the electron density rather than each individual wavefunction. This method starts by guessing an initial electron density. From this, the Coulomb potential due to the electrons is calculated at every point. Additionally, the exchange correlation potential due to antisymmetry is calculated. Then the Schrodinger's equation is solved for every electron at zero temperature and the density is recalculated by summing the individual densities. This is also iterated until the density converges. The underlying assumption behind the Kohn-Sham equations is that the electrons in the many-electron system do not affect each other. This simplifies the many-electron Schrodinger's equation at the cost of accuracy. [5]

There are many other approaches to solving the many-electron Schrodinger's equation such as the Configuration Interaction, Coupled Cluster, and Moller-Plesset Perturbation Theory, but these methods are very computationally heavy [5]. Another issue is that the exact functionals are unknown, which is why approximations are used.

B. **Approximations**

Local Density Approximation
One of the most fundamental approximations used in the Density Functional Theory is the local-density approximation (LDA). In this approach, the exchange correlation energy E_{XC} is given by (2).

$$E_{XC}[n] = \int d^3r\, n(r)\epsilon_{XC}\big(n(r)\big) \tag{2}$$

where $n(r)$ is the density at some location, ϵ_{XC} represents the exchange and correlation energies per electron in a homogenous electron gas with density $n[1]$. The LDA assumes that the electron gas is uniform. Although this simplifies the system, it tends to overestimate the exchange energy and underestimate the correlation energy in systems with non-uniform electron densities. [5]

Local Spin-Density Approximation
A way to improve LDA is by incorporating Pauli's exclusion principle, which states that no two electrons in an atom can occupy the same quantum state simultaneously. In other words, electrons with the same spin are distributed across orbitals which minimizes overlap. By applying this principle, we can separate electron densities from spin-up and spin-down electrons, which yields a more accurate estimate of the exchange and correlation energies, as shown in (3).

$$E_{XC}[n_\uparrow, n_\downarrow] = \int d^3r\, [n_\uparrow(r) + n_\downarrow(r)]\, \epsilon_{XC}\big(n_\uparrow(r), n_\downarrow(r)\big) \tag{3}$$

where $n_\uparrow(r), n_\downarrow(r)$ are the densities from spin-up and spin-down electrons respectively.

Generalized Gradient Approximation
There are other approximations that build on the LDA and LSDA to improve accuracy. The Generalized Gradient Approximation (GGA) incorporates the gradients of the electron density. While the LDA only considers local densities, the GGA accounts for spatial variation of the density, which significantly improves the accuracy of our approximation in non-uniform systems. [6]

The exchange correlation energy using GGA can be calculated using (4).

$$E_{XC}^{GGA}[n_\uparrow, n_\downarrow] = \int d^3r\, f(n_\uparrow, n_\downarrow, \nabla n_\uparrow, \nabla n_\downarrow) \tag{4}$$

where f is now a function of spin-up, spin-down electrons and also their gradients with respect to space.

As for Hybrid Functionals, one example is that the LSDA is sometimes used with the Quantum Monte Carlo, which is a random sampling method to solve many-body quantum problems.

C. Nudged Elastic Band Method

The Nudged Elastic Band Method (or NEB) was invented to find the minimum energy path between known reactants and products. NEB starts with an input of images – typically a linear pathway between the starting and ending states. To introduce the motivation for the NEB method, first we look at other methods to find the most efficient path, such as the Two-Dimensional LEPS Potential. The force acting on image is defined by (5) and (6). [7]

$$\vec{F}_i = -\hat{\nabla} V(\vec{R}_i) + \vec{F}_i^S \tag{5}$$

$$\vec{F}_i^S \equiv k_{i+1}(\vec{R}_{i+1} - \vec{R}_i) - k_i(\vec{R}_i - \vec{R}_{i-1}) \tag{6}$$

where V represents the potential, $\vec{F}_i^S$ represents the spring force, and $\vec{R}_i$ is the position vector. The spring force k_i is an artificial force added to maintain even spacing between images.

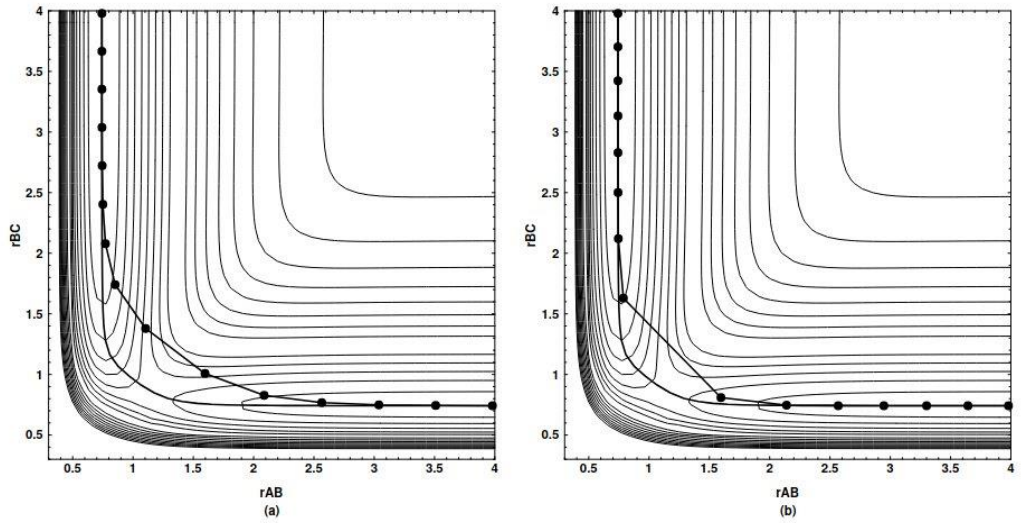

Fig. 1. Contour plot of the potential energy surface for three atoms whose movement is confined to 1 Dimension [7]

In the contour plot Fig. 1, the dotted line represents the most efficient path (MEP) calculated by the LEPS potential, and the non-dotted line represents the MEP using the NEB method. Notice how the MEP derived by the LEPS potential fails to capture the saddle point in both cases. In contrast, the MEP calculated by NEB is significantly more accurate, closely following the expected pathway.

The improvements of the NEB method are shown in (7) and (8). The NEB method optimized the energy of each image relative to neighboring images in an iterative process until the energy of the pathway has reached a specific threshold, and this is accomplished by "adding spring forces along the band between images and by projecting out the component of the force due to the potential perpendicular to the band" [8]. In other words, by projecting out the components perpendicular to the potential and parallel to the spring forces, we ensure that there are no forces that interfere with each other.

$$\vec{F}_i^0 = -\vec{\nabla} V(\vec{R}_i)|_\perp + \vec{F}_i^S \cdot \hat{\tau}_\parallel \hat{\tau}_\parallel \tag{7}$$

$$\vec{\nabla} V(\vec{R}_i)|_\perp = \vec{\nabla} V(\vec{R}_i) - \vec{\nabla} V(\vec{R}_i) \cdot \hat{\tau}_\parallel \hat{\tau}_\parallel \tag{8}$$

where $\hat{\tau}_\parallel$ is the unit tangent to the pathway.

III. Calculations and Results

A. Initial Energy Minimization

Calculations

The input files needed for both NEB and single-image minimization include crystal structure and pseudopotentials. The structure file (POSCAR) provides the coordinates for one supercell; the visualization of a structure file is provided in Fig. 2. We use a 6x6 supercell of graphene, with one carbon atom missing, and a vacuum chamber of 15 A in the z direction for the graphene. The coordinates of the atoms are fractional (from 0 to 1) and are then converted to position vectors by multiplying the coordinates with lattice vectors that skew the cell into the parallelogram prism seen in Fig. 2. Lattice vector details are provided in VII. Appendix. The pseudopotentials file (POTCAR) speeds up electronic structure calculations, using the project-augmented wave method, and frozen-core approximation [8]. Treating the rest of the atom minus the valence electrons as a singular core reduces equations, and the use of pseudo-potentials makes computing easier by necessitating fewer plane waves (functions that represent an electronic wave function in DFT as equations suitable for computing).

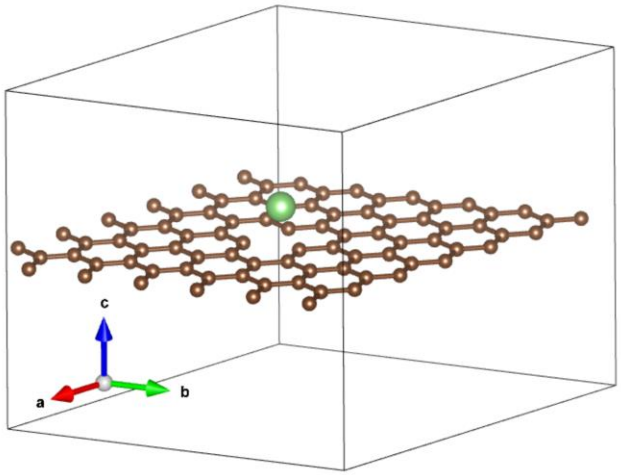

Fig. 2. Example 6x6 graphene supercell with lithium atom above carbon vacancy

Using the Self-consistency cycle, the cell is then minimized using this algorithm [8]:

1. An initial guess of electronic density to define initial Hamiltonian
2. Use matrix manipulation to obtain the N lowest eigenstates of the Hamiltonian
    a. N is the total number of QP orbitals in the calculation
3. Eigenstates and eigenvalues are used to compute the total energy of the system and create a new electronic density.
4. This is mixed with the old density to define a new Hamiltonian.
5. The cycle finishes when the total energy goes below the threshold, which is 10^{-4} eV in this case.

Results and Discussion

Attraction between carbon and metal atom will deform the graphene slightly and often push the metal atom higher. Fig. 3 shows the warping of the graphene supercell after the cell relaxation.

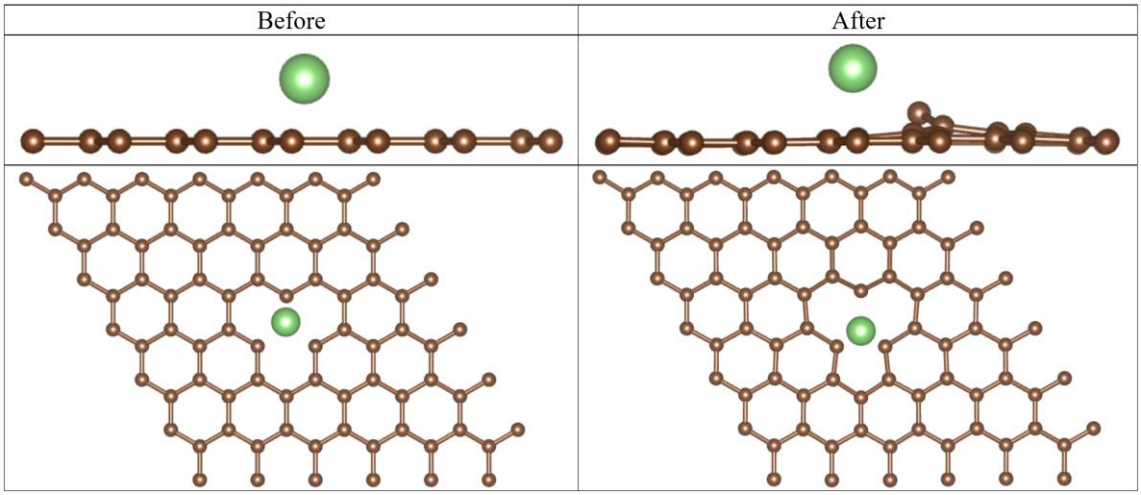

Fig. 3. Visualization of graphene supercell with lithium atom before and after energy minimization

More notably however is the discovery that slight adjustments in the atom's position above the monovacancy may affect the supercell after energy minimization. This is the case for when the atom is below the vacancy as well, but without loss of generality, we focus on when the atom is above. Table 1 depicts the fractional coordinates of a metal atom before and after energy minimization of the atom above a graphene monovacancy. The centered runs, highlighted in light blue, show clearly that the x and y coordinates do not change noticeably after minimization. On the other hand, the runs in the white tows start with off-centered atoms, and show a change after minimization. This is explored further with lithium in Fig. 4. The z coordinates after minimization appear mostly unaffected by the starting x and y position.

Table. 1 *Fractional Coordinates of Metal Atoms Before and After Energy Minimization Above Graphene Supercell*

Metal	X before	X after	Y before	Y after	Z before	Z after
Li	0.55555	0.55555	0.44444	0.44444	0.58000	0.61278
Li	0.56568	0.55112	0.46907	0.43570	0.60270	0.62248
Li	0.56000	0.55143	0.46000	0.43633	0.60270	0.62268
Fe	0.55555	0.55555	0.44444	0.44444	0.58000	0.59168
Fe	0.56568	0.55570	0.46907	0.44478	0.60270	0.59390
Mg	0.55555	0.55555	0.44444	0.44444	0.58000	0.62662
Mg	0.56568	0.55586	0.46907	0.44516	0.60270	0.62745
Cu	0.55555	0.55555	0.44444	0.44444	0.58000	0.60022
Cu	0.55769	0.55899	0.43098	0.44068	0.60270	0.59841

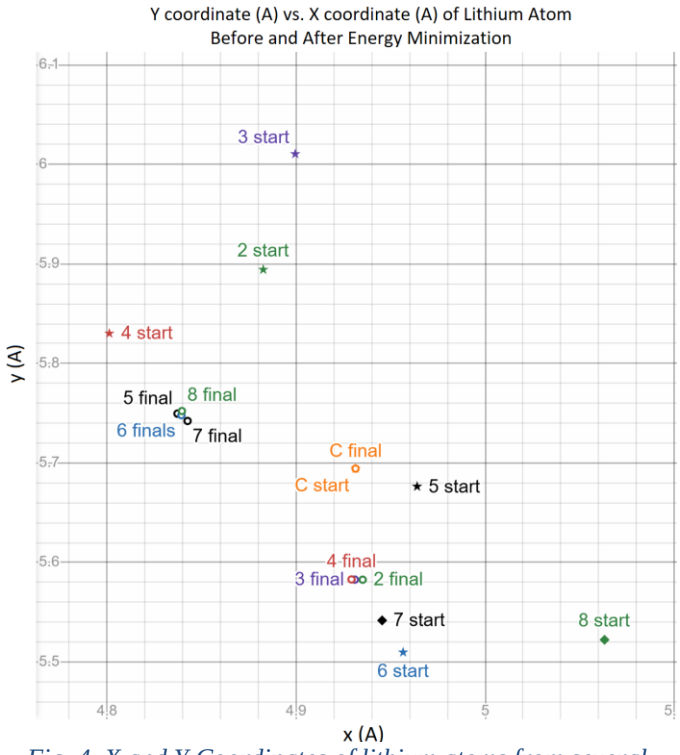

Fig. 4. X and Y Coordinates of lithium atoms from several energy minimization tests over graphene

In Fig. 4, the orange run is centered above the missing carbon, and the starting and final coordinates are near identical, as seen in Table 1 as well. Note that the coordinates plotted here are technically the end points of position vectors (using the skewing lattice vectors). By comparison, the off-center runs 2-4 converge to the same off-center location, and runs 5-8 converge to another off-center location. This suggests there are multiple energy minimums, which makes sense considering the rotational symmetry of the carbon vacancy and graphene structure itself.

There are two possible reasons the centered runs to not converge to a lower energy location: if the particle sits on the potential energy surface that is equal in every direction in value and/or gradient, then the program may assume it's already in the lowest energy point; this is essentially an energy trap that only exists at the centralized location. Secondly, if some value is exactly between two potential limit values, then the program does not allow it to converge to either value. Without noise in the simulation, there is nothing that will nudge the particle to one location or another, despite many iterations. The initial cell relaxation is significant because it does impact the NEB calculations, which is shown in the next section.

B. Nudged Elastic Band Calculations

Calculations

In order to perform an NEB calculation, we need an initial and final image that have both been minimized, as described in Section A. The initial image is the energy-minimized cell with the metal atom above, the final is that but with the metal atom below. Using 5 intermediate images – 7 including first and last image – we use the NEB method to find the minimum energy pathway of several atoms through a vacancy in graphene. To facilitate comparison with existing data, Table 2 shows the factors which we kept the same when running VASP based on [1].

Table 2. *Variable settings used in VASP for NEB calculations*

Variable	Value	Setting in VASP setup file
Kinetic Energy Cutoff	400 eV	ENCUT = 400
Spin Polarization	Account for spin polarization	ISPIN = 2
Energy Convergence Criterion	10^{-4} eV	EDIFF = 1.0E-04
Number of intermediate images	5	IMAGES = 5
K – Points	4 x 4 x 1	Specified in KPOINTS
Supercell Size	6 x 6	Specified in POSCAR
Vacuum Chamber	15A in z-direction	Specified in POSCAR

An important note is that the variation of NEB, called climbing image NEB, is often used instead. The focus of climbing NEB is the "convergence to a saddle point", which is done by moving up the potential surface along the pathway, and down perpendicular to it [9]. We used the regular NEB method as it may be more accurate when there is more than one energy peak, which is helpful if the energy landscape is unknown. Additionally, it is recommended to use 10-30 images, which would require significant parallel computing resources [7]. We use 5 images which is sufficient to get enough samples along the pathway, while being considerate of computing resources and time.

Results and Discussion

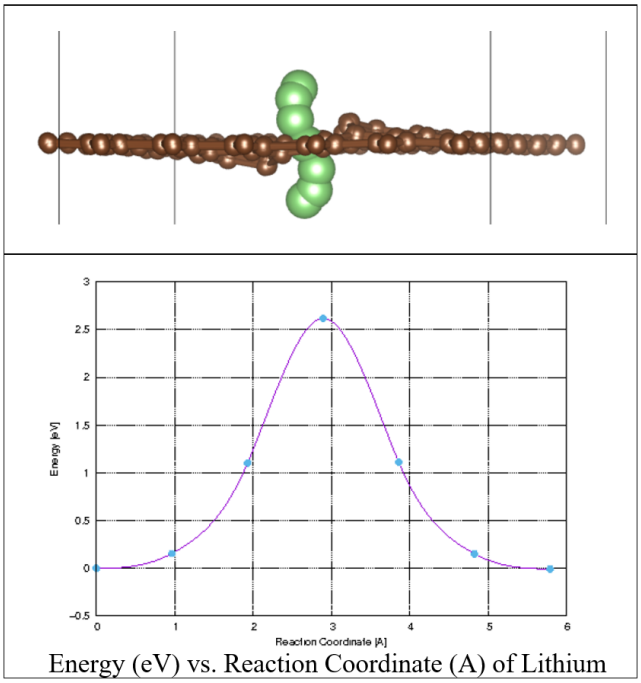

Fig. 5. Minimum energy pathway and energy for lithium intercalation

Fig. 5 depicts the minimum energy pathway of lithium through graphene, by combining all 7 images of the supercell. The energy barrier is plotted in eV vs. the reaction coordinates in Angstroms. The maximum energy is then 2.6eV, which is when the lithium atom is in line with the graphene sheet.

Fig. 6 shows the same data but when the lithium was previously minimized centered as opposed to off-centered. The second image from the bottom has a lower energy than the first/last images. Because the first and last images are fixed with NEB, the second and sixth images may assume the actual lowest energy position; this is especially visible with the 6th image, which is very close to the final image. This results in both energy dips and an asymmetrical plot and pathway. Instead of a maximum barrier of 2.6 eV, Fig. 6 shows 2.25 eV from the starting image.

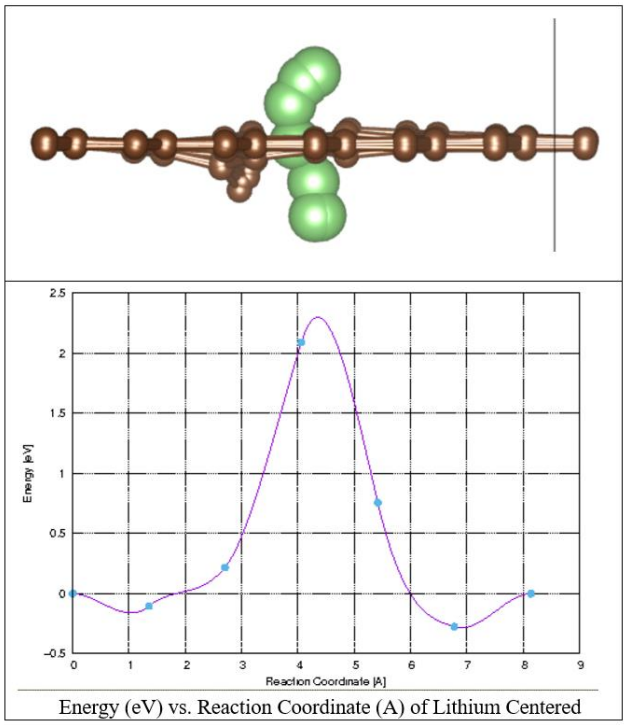

Fig. 6. Minimum energy pathway and energy for centered lithium intercalation

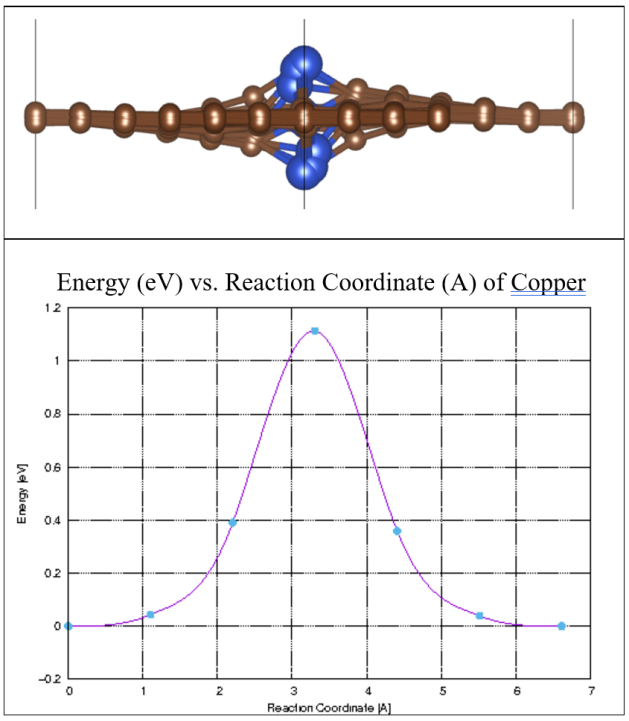

Fig. 7. Minimum energy pathway and energy for copper intercalation

Similarly, Fig. 7 depicts the pathway and energy barrier of copper, with an energy maximum of 1.1eV. When minimized centrally instead, the energy dips are existent though symmetrical, leading to a maximum barrier of 1eV instead of 1.1eV, shown in Fig. 8. This highlights the importance of minimizing the metal atoms off-center, although not previously noted from existing literature. In our calculations we use a mono-vacancy. We can compare this to larger vacancies, as done in other studies like the research paper by Y. Liu et. Al [1]. For vacancies of 1-3 carbon atoms, placing the atom in the center seemed to work. However, for 4-6 missing carbon atoms, the copper and iron tended to attach to the edge of the vacancies, with metal-carbon bonds. They noted that the ability for the atoms (Cu, Rb, Pt, Fe) to penetrate the graphene significantly reduced when the vacancy was larger than one carbon atom missing. Lastly, it seems that the limiting factor for intercalation is the detachment or second half of the process. The nudged elastic band method shows us the minimum energy pathway, which may be unexpected, like the spiral or S-shaped paths that the metal atoms take through the vacancy in the graphene sheet.

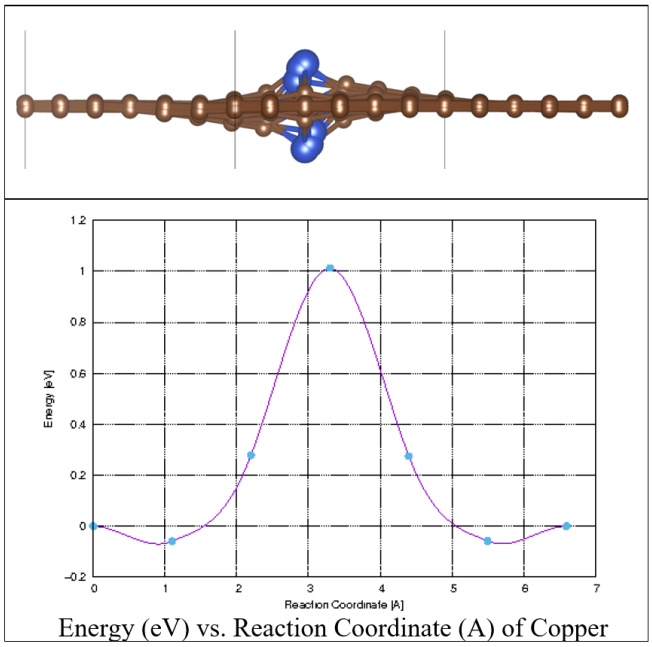

Fig. 8 Minimum energy pathway and energy for centered copper intercalation

IV. Applications

A. Tuning and Semiconductors

Gr/ir(111) is one monolayer of graphene deposited on (111) oriented iridium. Due to iridium's "high crystalline quality and extremely low surface roughness", the graphene layer can be synthesized with chemical vapor deposition with almost complete coverage [10]. This is a close approximation to free-standing graphene layers that are used in the VASP experiments. In a study by Y. Dedkov and E. Voloshina, it was discovered that the intercalation of copper atoms in gr/ir(111) does in fact alter the electric properties of graphene. Specifically, it induced n-doping in the graphene, with a 0.69 ± 0.01 eV energy shift of the Dirac point of graphene [3]. The Dirac points are the points of the cones in Fig. 9 (a), and the vertices of the hexagon in (b) [4]. These points represent when the energy gap between the conduction and valance band disappear, or becomes 0eV. Interestingly, this energy gap at the Dirac points opened to 0.36 ± 0.01 eV for the graphene π states [3]. This transforms graphene from a semimetal to a semiconductor because electrons can no longer travel freely between the valence and conductions bands. Additionally, the intercalation of oxygen on graphene deposited in (0001) oriented rubidium results in p-doping [3]. It suffices to say that intercalation alters graphene's bandgap, and that studying intercalation/diffusion of metal atoms aids in purposefully tuning this bandgap. Findings in both physical experiments and DFT analysis of graphene can also be applied to other 2D materials, such as Li_xCoO_2 [11].

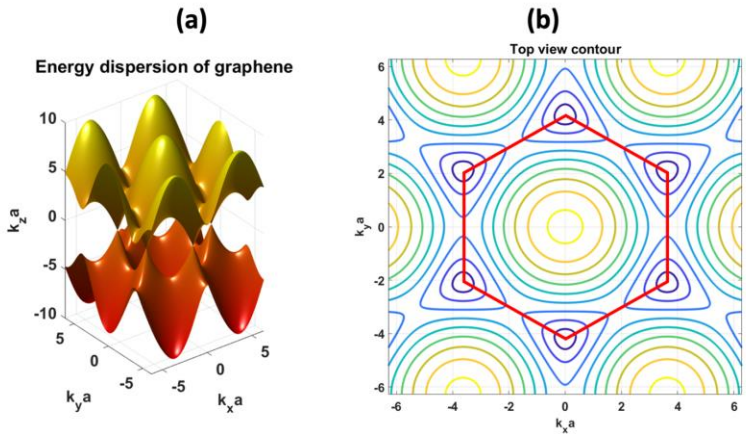

Fig. 9. (a) Band structure of graphene. (b) Contour plot of the band structure vs. the wave vector space (k_x, k_y) [4]

B. Lithium Ion Batteries

Lithium-ion batteries work by intercalating lithium+ through solid materials, to charge and discharge. Due to high demand and environmental concerns, researchers constantly seek ways to improve lithium ion batteries. Ershadi et al. developed a process for creating graphene oxide nanosheets with ethylenediamine to regulate the structure. By N-doping the graphene and using it as a cathode in the battery, the battery showed "remarkable rate potential, promising reversible capacity, and long-life cycling stability" [2, page 9]. Additionally, S-doped graphene also provided long performance for the batteries and were more economic and lighter/more portable [2]. Studying how to tune the doping concentration of graphene potentially via intercalation could therefore improve the battery performance and reversibility of lithium-ion batteries. In a similar vein, other 2D materials are being proposed as a cathode for lithium-ion batteries. 2D Hybrid halide perovskite is being considered because of its 3.2 open-circuit voltage [12]. While the electrochemical performance was impressive, "a poorly establish reaction pathway highlights the need for an in-depth study" [12, page 1819]. When studying the effectiveness of new materials like $CsPbBr_3$, $LiTiO_3$, and CH_3NH_3PbI, in Lithium-Ion batteries, these kinds of calculations prove to be insightful.

V. Conclusions

The Density Functional Theory and the approximations that follows provide solutions and simplifications that make solving quantum systems computationally feasible. Using DFT, the nudged elastic band method was created to find the minimum energy pathway between two states. With parallel computation and quantum mechanics simulation VASP, we calculated the minimum energy pathway of metal atoms through a sheet of graphene with one vacancy. When minimizing the first and last image of the pathway, it is important to start with the metal atom off-center. Our experiments show that the nudged elastic band method is less effective when the metal atom is centered; it may cause inaccurate energy dips or asymmetrical pathways. Analysis of the computing method shows it may be due to atom existing on the potential energy surface such that the gradient and values are equal in all directions. It could also be that the lack of noise in the simulated system does not allow the atom to converge to two equally lower energy points. Both lithium and copper form a spiral or S-shape pathway through the monovacancy, with lithium having an energy barrier of 2.6eV, and copper with 1.1eV. Further extrapolated, this field of research is relevant to both semiconductors and lithium-ion batteries. Intercalation of metal atoms has been shown to induce n-doping in graphene and create a bandgap transforming the semimetal into a semiconductor. Additionally, the study of both atom intercalation through graphene and more complex 2D materials provides promising insight into its use in lithium-ion batteries. 2D materials is an interesting avenue that highlights the ability to translate pure math into engineering new technology.

VI. References

[1] Y. Liu, X. Liu, C. Wang, et. Al, "Mechanism of Metal Intercalation under Graphene through Small Vacancy Defects," *Journal of Physical Chemistry,* vol. 125, pp. 6954-62, 2021.

[2] A. Ali, F. Liang, et. Al, "The role of graphene in rechargeable lithium batteries: Synthesis, functionalization, and perspectives," *Nano Materials Science*, Jul. 2022.

[3] Y. Dedkov, E. Voloshina, "Spectroscopic and DFT studies of graphene intercalation systems on metals," *Journal of Electron Spectroscopy and Related Phenomena*, vol. 219, pp. 77-85, Dec. 2016.

[4] M.P. Anantram, S. Daryoush. *Quantum Mechanics for Engineers and Material Scientists.* Singapore, World Scientific Publishing Company, Feb. 2024.

[5] D. Bagayoko, "Understanding density functional theory (DFT) and completing it in practice," *AIP Advances 4,* vol. 4, Dec. 2014.

[6] J. Perfew, K. Burke, M. Ernzerhof, "Generalized Gradient Approximation Made Simple," *Phys. Rev. Lett.,* vol. 77, Oct. 1996.

[7] H, Jonsson, G. Mills, K. Jacobsen, "Nudged elastic band method for finding minimum energy paths of transitions," *Classical and Quantum Dynamics in Condensed Phase Simulations,* World Scientific, 1998.

[8] "VASP Wiki". *VASP Manual,* online. https://www.vasp.at/wiki/index.php/The_VASP_Manual.

[9] G. Henkelman, B. Uberuaga, H. Jonsson, "A climbing image nudged elastic band method for finding saddle points and minimum energy paths," *Journal of Physical Chemistry,* vol. 113, pp. 9901-04, Dec. 2000.

[10] A. Pandey, K. Krausert, et. Al, "Single orientation graphene synthesized on iridium thin films grown by molecular beam epitaxy," *Journal of Applied Physics,* vol. 120, Aug. 2016.

[11] PG. Bruce, "Solid-state chemistry of lithium power sources," *Chem Inform,* vol. 28, 1997.

[12] J. Dawson, A. Naylor, et. Al, "Mechanisms of Lithium Intercalation and Conversion Processes in Organic-Inorganic Halide Perovskites," *ACS Energy Letters*, vol. 8, pp. 1818-24, Feb. 2017.

VII. Appendix

Table i. *Lattice vectors used for graphene 6x6 supercell (Angstroms)*

14.7958183288999994	0.0000000000000000	0.0000000000000000
-7.3979108706999996	12.8135535575000006	0.0000000000000000
0.0000000000000000	0.0000000000000000	15.0000000000000000

These vectors in Table i leave the Z-direction unchanged (other than scaling by 15 Å), while transforming a unit square into a parallelogram in the horizontal direction. The position vector $\vec{R}$ for any single atom is calculated using (ii), with a magnitude given in Angstroms.

$$\vec{R} = x\overrightarrow{a_1} + y\overrightarrow{a_2} + z\overrightarrow{a_3} \quad \text{(ii)}$$

where $\overrightarrow{a_1} \approx \langle 14.796,\ 0,\ 0\rangle, \overrightarrow{a_2} \approx \langle -7.398,\ 12.814,\ 0\rangle, \overrightarrow{a_3} \approx \langle 0,\ 0,\ 15\rangle$, and x, y, z are the fractional coordinates of the atom.